sustainability

MDPI

Essay

A Numerical Method for Evaluating the Collapse of High-Steep Scarp Slopes Based on the Bonded Block Model–Discrete Fracture Network Model

Zening Sun [1,2], Shili Qiu [1,*], Siquan Yan [3] and Zaiquan Wang [2]

[1] State Key Laboratory of Geomechanics and Geotechnical Engineering, Institute of Rock and Soil Mechanics, Chinese Academy of Sciences, Wuhan 430071, China; 18661674387@163.com
[2] School of Science, Qingdao University of Technology, Qingdao 266033, China
[3] Yellow River Engineering Consulting Co., Ltd., Zhengzhou 450003, China
* Correspondence: slqiu@whrsm.ac.cn

Abstract: Geotechnical engineering works in deep-incised valleys or open-pit mining areas often encounter high-steep scarp slopes with a slope angle greater than 75°. This type of slope directly threatens the safety of construction personnel, so assessing their stability is essential to ensure construction safety. The natural geometry of high-steep scarp slopes possesses complexity in terms of geometric morphology, structural features of rock mass, and occurrence mechanisms of collapse. There is little research and less emphasis on the evaluation of the collapse risk of high-steep scarp slopes. In particular, the fracture of intact rock or rock bridges is generally ignored in the analysis of collapse processes. A bonded block model (BBM)–discrete fracture network (DFN) coupling characterization model for the high-steep scarp slope is proposed based on a high-steep scarp slope containing dominant joint sets on the left bank of the dam site of the Huangzangsi Water Conservancy Project (Qinghai Province, China). By using the model, the complex geometric forms of the surface of the high-steep scarp slope are quantified, and the fracture process of falling rock masses as well as the controlling effect of dominant joints on the collapse of the scarp slope are revealed. A strength reduction method based on the BBM–DFN model is constructed, and the safety factor of the collapse-prone scarp slope is evaluated. The research results show that (1) the BBM–DFN model can be used to describe the local collapse process; (2) the occurrence of dominant joints plays an important part in controlling the collapse process; (3) there are differences in the safety factor of the scarp slope with different coupling methods; the collapse and failure modes also differ. For safety considerations, the safety factor of the scarp slope on the left bank of the dam site area is determined to be 1.85. The research findings can be used to guide the safety assessment of high-steep scarp slopes and the formulation of both collapse risk prevention and control measures to ensure construction safety in high-steep scarp slope areas.

Keywords: high-steep scarp slope; bonded block model–discrete fracture network coupling; safety factor for high-steep scarp slope; collapse risk analysis

Citation: Sun, Z.; Qiu, S.; Yan, S.; Wang, Z. A Numerical Method for Evaluating the Collapse of High-Steep Scarp Slopes Based on the Bonded Block Model–Discrete Fracture Network Model. *Sustainability* **2023**, *15*, 15672. https://doi.org/10.3390/su152115672

Academic Editors: George D. Bathrellos and Hariklia D. Skilodimou

Received: 25 July 2023
Revised: 27 October 2023
Accepted: 30 October 2023
Published: 6 November 2023

1. Introduction

High-steep scarp slopes generally refer to free slope surfaces that are higher than 30 m, have a slope angle greater than 75°, and developed in deep-incised valleys or mountainous areas. In engineering construction, construction structures such as road surfaces, open-pit mining areas, and auxiliary buildings are generally constructed below or within a scarp slope. Collapse of such high-steep scarp slopes directly threatens the safety of builders and even causes serious accidents, so a safety assessment is crucial for ensuring construction safety; otherwise, it will cause heavy economic losses and personnel safety issues [1]. Table 1 summarizes some typical collapse cases from high-steep scarp slopes around the world and the hazards posed by them; collapse of high-steep scarp slopes directly threatens

the safety of construction personnel, often halting large engineering projects, resulting in huge economic loss and even failure of engineering construction. However, stability evaluation regarding the collapse of high-steep scarp slopes has been seldom studied or paid attention to due to the complexity of the natural geometry of such slopes, the structural features of such rock masses, and the mechanisms of collapse.

Table 1. Collapse cases of high-steep scarp slopes around the world (incomplete statistics).

Location	Lithology	Slope Height/m	Slope Angle/°	Joint Development	Causes	Hazard
Cenxi Tianma Stone Industry Co.,Ltd., Guangxi Province, China [2]	granite	175	60	Development of two dominant joint sets	Reduction in joint surface strength	4 persons died and 1 person obtained minor injuries.
Honglianchi Iron Mine in Hefeng, Hubei Province, China [3]	Micaceous shale	100	60	Development of three dominant joint sets	Karst dissolution, mining, and a rainstorm	Village roads were blocked by collapsed deposits over a length of 150 m
Jiguanling in Wulong County, Chongqing Province, China [4]	Limestone	200	60–70	Development of two dominant joint sets	Rock properties	Destruction and sinking of 5 vessels, with over 20 casualties.
Zhaojiagou Village, Zhenxiong County, Yunnan Province, China [5]	Sandstone	100	50–80	Development of three dominant joint sets	Persistent rainfall	46 casualties, 63 houses were destroyed, and 500 mu of farmland was damaged
Yanchihe phosphate mine in Yuan'an County, Hubei Province, China [6]	Dolomite	125	80	/	Deformation of above mountain due to phosphate ore mining	307 died, and lots of equipment was damaged
Zongling Town, Nayong County, Guizhou Province, China [7]	Limestone and Sandstone	40	70	Development of single dominant joint sets	Heavy rainfall and weathering processes	39 people dead, 5 missing, and an additional 14 people injured.
Minas Geras, Brazil	sedimentary rock	20	90	/	The rain causes the cohesion between the rocks and the internal friction angle decrease.	7 persons dead, 20 missing and 32 injured

A review of numerous studies has shown that the following three problems exist in research on collapse of steep scarp slopes:

Key controlling factors for the collapse of steep scarps are misunderstood. Although researchers like Fang Chuanfeng et al. [8] introduced the PFC-DFN model into the study of natural collapses in mines, there is little research into the progressive collapse process of steep scarps. Existing research focuses more on the controlling effect of the instability of blocks with structural planes or joint sets on the collapse. However, many collapse cases of high-steep scarp slopes have shown that the key controlling factor determining collapse failure is the fracture process of an intact rock mass and intact rock bridges between joints. These include: (1) Local intact rock or rock between blocks under the self-gravity of the block itself. Alberto Bolla et al. [9] investigated the mechanical behavior and internal rock mass damage of the unstable slope before the collapse, and obtained the collapse mechanism of high-steep scarp slope under the influence of the self-gravity

of the block itself. (2) External disturbances (such as seismic waves, engineering blasting vibrations, construction machinery vibrations, etc.). Cui Fangpeng et al. [10] studied the dynamic coupling conditions of the Tangjiashan slope in Beichuan using the discrete element technique. Chen Ming et al. [11] studied the influence of blasting vibration speed on the stress state of the slope, based on wave theory. (3) Strength degradation of rock masses after weathering. L. Borrelli et al. [12] studied the influence of different weathering grades on the instability of a high-steep scarp slope. Xu Jiang et al. [13] focused on the Fengdu Mingshan landslide mass and investigated the influence of weathering erosion on landslide instability. (4) Rainwater-induced fissure water splitting. Nathalia Silva Oliveira et al. [14]—based on the Rio de Janeiro mountainous area in Brazil—studied the impact of rainfall and mountain landslides. Do Ngoc Ha et al. [15] simulated the large-scale collapse of limestone slopes induced by torrential rainfall at Khanh Waterfall in Hoa Binh Province, Vietnam, using 3DEC 5.0. This simulation provides indicators for assessing its hazard.

Failure criteria for the collapse of high-steep scarp slopes remain imperfect. Several failure criteria are available for the stability assessment of steep scarps: (1) Convergence of numerical calculation: Griffiths D V et al. [16] proposed replacing traditional limit equilibrium methods with finite element stability analysis methods. Naeij Morteza et al. [17] introduced a slope strength reduction method based on the iterative finite element method (FEM/I). (2) Abrupt change of displacement at characteristic points. Wang Dong et al. [18] found that the displacement discontinuity at critical points is more suitable for stability analysis when steep cliffs undergo significant deformations. Zhao Shangyi et al. [19] proposed that rockfall and the transition of rocks from a static to a dynamic state, accompanied by large and unbounded displacements, are characteristic features of failure. (3) Coalescence of plastic zones. Majid T. Manzari et al. [20] and Luan Maotian et al. [21] suggested that the plastic zone penetration method is applicable as a discriminative approach. However, these methods are extensions of traditional slope stability assessment methods and may not fully consider the specific hazards caused by rock mass collapse in steep cliffs. However, they are extensions of traditional criteria for slope stability to steep scarps and do not consider hazards caused by the avalanche of unstable rock bodies specific to high-steep scarp slopes.

The controlling factors of the collapse of high-steep scarp slopes are not studied comprehensively. Previous research has found that various parameters may influence the collapse of steep scarps: Mahendra Acharya et al. [22] took shear stiffness and normal stiffness as key factors, and introduced them to a collapse model for simulation. Bai et al. [23] used discrete element software for the numerical simulation of high-steep scarp slopes and concluded that the poor stability of surface blocks and controlling blocks on these slopes is likely to cause overall failure. Wang et al. [24] simulated the natural collapse of ore-bearing rock based on the particle flow code (PFC), which provides an idea and method for later PFC study. Luirei Khayingshing et al. [25] found that wedge failure, sliding (bedrock and debris), and toppling are the primary types of failure mechanisms, of which wedge-failure-induced landslides account for the maximum. Bi et al. [26] proved that the cohesion of the rock affects rockfall through the use of the discrete element method. Moein Salavati et al. [27] conducted a study on the influence of rock disturbance coefficients on the SRF (Slope Stability Safety Factor) of slopes with different inclinations. Shiferaw Henok Marie [28] selected a slope with steep scarps, degree of fragmentation of unstable rock, dip angle of beddings, and thickness of strata as factors influencing its collapse. Zhang et al. [29–34] conducted research on the failure criteria of rocks. Chen et al. [35–38] conducted research on the failure criteria of jointed rocks. However, they did not systematically analyze the collapse of high-steep scarp slopes, so either the chosen parameters were inadequate or the analytical process was inapplicable to judging the stability of steep scarps, thus failing to guide engineering design and safe construction.

In view of this, high-steep scarp slope engineering with dominant joint sets at the left bank of the dam site of Huangzangsi Water Conservancy Project (Qinghai Province, China) was studied here. By applying the block discrete element method, a bonded block model (BBM)–discrete fracture network (DFN) coupling characterization model for the high-steep

scarp slope was established. In addition, three reduction methods for mesoscopic joint parameters in the BBM–DFN model were proposed, as well as the targeted convergence and failure criteria for the high-steep scarp slope. These methods were used to elucidate the collapse mechanism of the high-steep scarp slope with a slope angle larger than 80° containing dominant joints under natural conditions due to both rock fracture and presence of dominant joints.

2. BBM–DFN Coupling Discrete Element Analysis Method for the Stability of High-Steep Scarp Slopes

2.1. BBM–DFN Model for High-Steep Scarp Slopes

High-steep scarp slopes are characterized by a slope angle steeper than 75°, an altitude difference of 100 m, abundant surface deposits, development of many dominant joints, and severe weathering and erosion. Considering these, a decrease in cohesion of intact rock blocks and distribution of numerous dominant joints can induce collapse of steep scarps. To study the controlling effects, the fracture process of a rock mass, and the dominant joints on the collapse of steep scarps, the BBM–DFN model is used to analyze the collapse risk of high-steep scarp slopes with complex geometry.

2.1.1. BBM Model

The BBM refers to using tetrahedra to split an intact block into a block model that is composed of numerous tetrahedral particles. High-steep scarps consist of rock, each of which is interlocked with surrounding blocks, implying that the macroscopic mechanical behaviors of steep scarps are directly related to the contact properties between rock blocks, including the stiffness, cohesion, tensile strength, and internal friction angle of contact surfaces. To study influences of the fracture of a whole rock block on the collapse risk of high-steep scarps, the BBM is used here to divide a high-steep scarp slope into lots of independent rock blocks and explore the mesoscopic bonding parameters of the blocks.

2.1.2. DFN Model

In the collapse process of high-steep scarp slopes, dominant structures cutting the rock mass are involved; these are important factors that control the collapse process, making it necessary to introduce dominant structural planes and their network in the characterization model of the rock mass. To this end, the DFN method is used to study the controlling factors of the fracture of rock bridges between dominant joints for the collapse of high-steep scarp slopes. The modeling of the DFN involves two situations: (1) the definitive DFN model is used for characterization if joints in the high-steep scarp slope are fully investigated; if geometrical parameters of structural planes including the number, occurrence, and spacing are clear; if there are only a few structural planes; (2) if dominant structural planes are of statistical significance and their number, occurrence, and spacing can be quantified through statistical distribution; or if there are multiple networks formed by structural planes, which are difficult to model using the definitive method. The random DFN model is used for characterization.

2.1.3. Coupling of the BBM and DFN Models

To simultaneously study the controlling effects of the interaction force between rock and the fracture of rock bridges between dominant joint sets on the collapse process of high-steep scarp slopes, the BBM is coupled with the DFN (Figure 1). At first, an overall model is constructed, which is then divided into the BBM model using tetrahedral blocks. At the same time, the random DFN model or the definitive DFN model is established according to joint or fracture parameters. Finally, the established DFN model is nested within the BBM model to form the coupled BBM–DFN model.

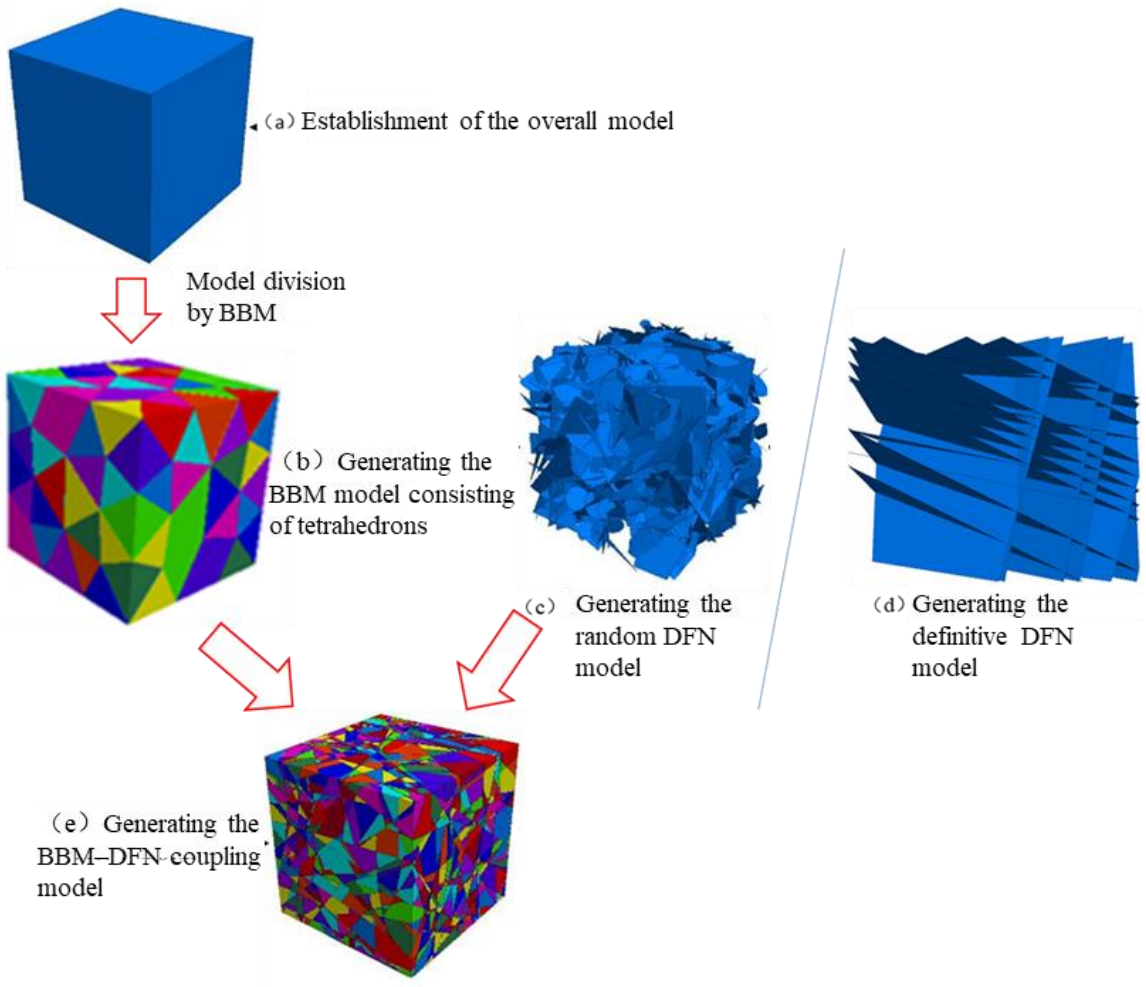

Figure 1. Schematic diagrams of the coupling process of the BBM-DFN model. (**a**) Establishment of the overall model; (**b**) Generating the BBM model consisting of tetrahedrons; (**c**) generating the random DFN model; (**d**) Generating the definitive DFN model; (**e**) Generating the BBM-DFN coupling model.

2.2. Strength Reduction Methods for Collapse Based on the BBM–DFN Model for High-Steep Scarp Slopes

Stability analysis of high-steep scarps generally uses methods including the limit equilibrium slice method [39,40] and strength reduction method [41]. Traditional reduction methods for cohesion and the internal friction angle of intact rock generally fail to meet the demand for simulating the fracture process of intact rock and intact rock bridges between joints during the collapse of high-steep scarp slopes based on the coupled BBM–DFN model. Therefore, three reduction methods aiming at parameters of mesoscopic joints between blocks in the BBM–DFN structural characterization model for rock blocks are proposed:

(1) In the reduction method considering the internal friction angle and cohesion of mesoscopic joints between blocks in the BBM–DFN model (CF-RM), failure of a high-steep scarp is mainly shown as shear failure along the joint planes in rock. Khan Muhammad Israr et al. [42] suggested considering the trend of safety factor variation with changes in shear strength when analyzing slope stability.

(2) The reduction method considering internal friction angle, cohesion, and tensile strength of mesoscopic joints between blocks in the BBM–DFN model (CFT-RM) holds that failure of rock in actual high-steep scarp engineering is compression-shear combined failure, so the tensile strength parameter of joints is incorporated into the reduction parameters. Pantelidis Lysandros et al. [43] found that tensile strength has

a significant impact on slope stability under three-dimensional conditions. Dowon Park [44] obtained the relationship curve between tensile strength and slope stability factor.

(3) The reduction method for the internal friction angle, cohesion, and deformation parameters of mesoscopic joints between blocks in the BBM–DFN model (CFD-RM) considers not only strength parameters, but also deformation parameters of the high-steep scarp degrade, so the deformation parameters are incorporated in the reduction parameters. Yu Cheng Zhang et al. [45] proposed that the main result is the safety factor of the slope, but in the calculation process, the nonlinearity of the soil was not actually considered, making it difficult to obtain a realistic deformation field. However, using the elastic-plastic strength reduction method based on the deformation modulus can yield a more realistic deformation field.

2.2.1. CF-RM

According to the CF-RM, rock failure of a high-steep scarp slope is mainly dominated by shear failure between joint planes in the rock. For the coupled BBM–DFN discrete element model, the shear strength of discontinuous contact surfaces is mainly related to the cohesion and surface morphology of contact surfaces, as well as the stress on joint planes; reduction formulas are given by (Equations (1) and (2)):

$$c_i = \frac{c_0}{I} \tag{1}$$

$$\varphi_i = \arctan[\tan(\varphi_0)/I] \tag{2}$$

where c_0 and φ_0 refer to the original cohesion and internal friction angle of mesoscopic joints, respectively; c_i and φ_i represent the reduced cohesion and internal friction angle of mesoscopic joints, respectively; and I denotes the strength-reduction coefficient.

2.2.2. CFT-RM

According to reduction formulas for the internal friction angle and cohesion of mesoscopic joints between blocks in Section 2.2.1, the CFT-RM further considers that geotechnical materials in slope engineering are generally under three-dimensional (3D) compressive stress, so the failure mode should entail a combined compression-shear failure. The measured tensile strength obtained by Wu et al. [46] and Yuan et al. [47] in their research on parameter reduction of rock should satisfy (Equation (3)):

$$f < \frac{2c\cos\varphi}{1+\sin\varphi} \tag{3}$$

According to the relation, the measured tensile strength of mesoscopic joints in the BBM–DFN model should satisfy the following Equations:

$$\alpha f_{ti} < \frac{2c_i\cos\varphi_i}{1+\sin\varphi_i} \tag{4}$$

$$\alpha < \frac{2c_0\cos\varphi_0}{1+\sin\varphi_0}\frac{1}{f_t} \tag{5}$$

where c_0, φ_0, and f_t refer to the original cohesion, internal friction angle, and tensile strength of mesoscopic joints, respectively; c_i, φ_i, and f_{ti} represent the cohesion, internal friction angle, and tensile strength of mesoscopic joints after reduction to the i-th step, respectively; and α is a constant.

2.2.3. CFD-RM

According to reduction formulas for the internal friction angle and cohesion of mesoscopic joints between blocks in Section 2.2.1, CFD-RM considers that deformation in most

high-steep scarps ended after formation in nature if not considering the external force, so the slope is in a stable state. Failure of steep slopes is mainly triggered by external actions, such as rainfall, weathering, and earthquakes, which also induce changes of the deformation parameters while reducing strength or increasing load. According to Zheng et al. [48], Poisson's ratio and the internal friction angle of rock should satisfy Equation (6):

$$\sin \varphi \geq 1 - 2\nu \tag{6}$$

Based on this relationship, the deformation parameters in the coupled BBM–DFN discrete element model should satisfy the following formulae:

$$\nu_i = \frac{1}{2}(1 - \frac{\sin \varphi_i}{\beta}) \tag{7}$$

$$\beta = \frac{\sin \varphi_0}{1 - 2\nu_0} \tag{8}$$

$$E_i = \frac{E_0 \nu_0}{\nu_i} \tag{9}$$

where ν_0, φ_0, and E_0 refer to the original Poisson's ratio, internal friction angle, and elastic modulus of joints in geotechnical materials, respectively; ν_i, φ_i, and E_i represent the Poisson's ratio, internal friction angle, and elastic modulus of mesoscopic joints after reduction to the i-th step, respectively; and β is a constant.

2.3. Failure and Convergence Criteria Based on the BBM–DFN Model of High-Steep Scarp Slopes

Based on the BBM–DFN model of high-steep scarps and the three different reduction methods, it is a necessity to choose reliable failure and convergence criteria. The criteria of strength reduction methods generally fall into three types: abrupt changes of displacement at characteristic points, coalescence of plastic zones, and convergence of numerical calculation. The research focuses on the collapse of the high-steep scarp surface. Therefore, it is more appropriate to arrange sufficient monitoring points for displacement on the free face of the high-steep scarp to monitor abrupt changes in the displacement curve, and combine these with data pertaining to the number of cracks, which can be used as the criterion for collapse.

In the calculation process, the high-steep scarp in the BBM–DFN model is composed of discontinuous blocks, which may fail to converge due to falling of local blocks. Therefore, determining the judgment method for convergence of numerical calculation—that is, when the calculation terminates—is a key problem. Based on the statistical analysis of the displacement data, it was proposed to use the condition when the curve for the ratio of the standard deviation of displacement at characteristic points (arithmetic square root of variance) to the average displacement approaches the horizontal as the criterion for convergence. Here, the ratio is the coefficient of variance (CV), whose curve is shown in Figure 2. When the CV curve tends to be parallel to the horizontal asymptote, it suggests that the dispersion degree of displacement at monitoring points remains unchanged. That is, the failure process of the rock has ended, and the calculation converges.

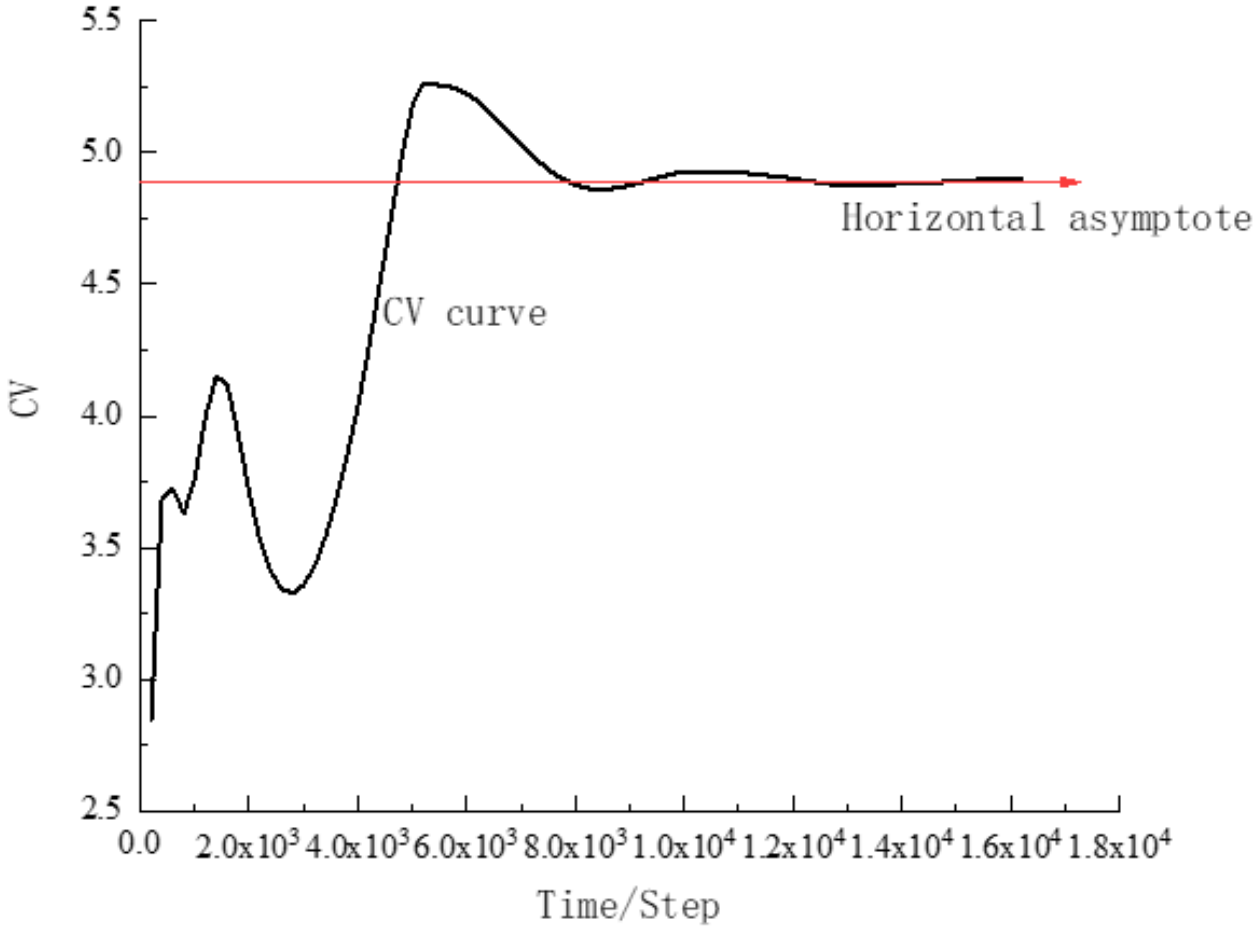

Figure 2. Sampling map of the CV of the displacement at the monitoring points.

3. Establishment of the BBM–DFN Model for the High-Steep Rocky Scarp Slope on the Left Bank of the Dam Site of the Huangzangsi Water Conservancy Project and Simulation Schemes

3.1. Project Overview

The dam site of Huangzangsi Water Conservancy Project is constructed on the trunk stream of the Heihe River 11 km downstream from Huangzangsi Village, with a drainage area of 7648 km^2 and a mean annual natural runoff of 1.259×10^9 m^3. The high-steep scarp slope on the left bank of the dam site lies above an altitude of 2690 m, as shown in Figure 3. The bedrock of the high-steep scarp is composed of chlorite, muscovite, quartz, and schist, and the slope angle is between 60° and 80°. The slope shows an altitude difference as large as 110 m, and is steep, on which there are large amounts of deposits. Two dominant joint sets develop in the slope: with an occurrence of 90°–110°∠ 30°∼40°; joint set J is characterized by fluctuant and rough joint planes, and most sections are closed without filling (albeit with some local rock debris infill). The joint set extends to great length and includes five joints. Joint set L has an occurrence of 75°–80°∠ 60°∼70°, in which the joint planes are fluctuant (or straight) and rough, filled with rock debris, or not filled. There are five large joints in the joint set.

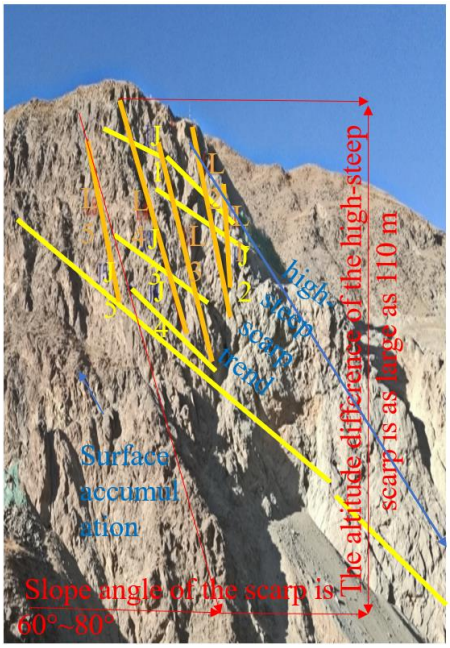

Figure 3. Geological condition and dominant joint distribution in the high-steep scarp on the left bank of the dam site of Huangzangsi Water Conservancy Project.

3.2. Establishment of a Planar BBM Model on the High-Steep Rocky Scarp Slope

Based on the engineering reality of the high-steep rocky scarp slope on the left bank of the Huangzang Temple hydropower project, a planar model was established to study the failure mode of the high-steep rocky scarp slope without discontinuous fracture networks (DFN). By determining the position of the slip surface, the minimum depth of the model was established when creating the three-dimensional model. Therefore, sections with slopes greater than 80° were selected, and a 1-m-thick BBM model was created in the 3DEC 5.0 (Figure 4a) with boundary conditions (Figure 4b). The highest elevation of the model is 63 m, and the widest part at the bottom is 28 m.

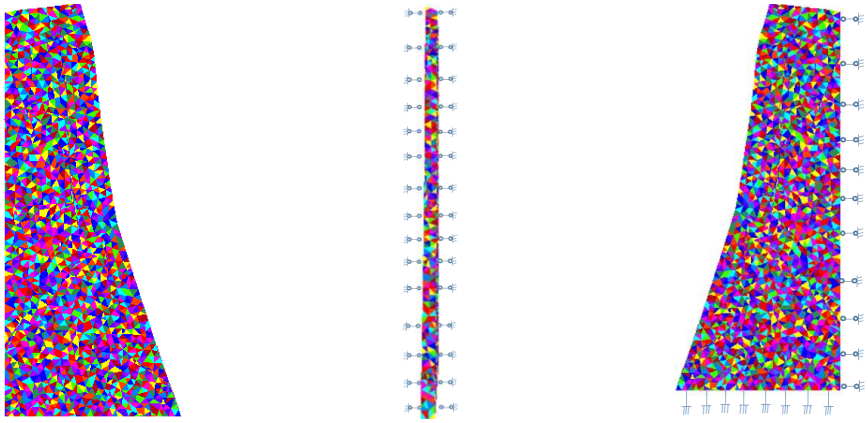

(**a**) (**b**)

Figure 4. High-steep scarp slope model on the left bank of the dam site of Huangzangsi Water Conservancy Project and boundary conditions. (**a**) Local model for the high-steep scarp slope. (**b**) Boundary conditions of the Planar model of the high-steep scarp slope.

3.3. Establishment of the BBM–DFN Model for the High-Steep Rocky Scarp Slope

The BBM–DFN coupling model is built by using 3DEC 5.0 based on the practical engineering work undertaken on this high-steep scarp slope with dominant joint sets on the left bank of the dam site of Huangzangsi Water Conservancy Project to evaluate stability

of the slope. Controlling factors for the collapse of the scarp slope are explored to provide reference for subsequent construction of the dam body and the reinforcement of the slope. Because the research mainly focuses on surface collapse of the high-steep scarp, a model for the studied high-steep scarp slope is built based on distribution characteristics of joints in the slope containing complex rock structures (Figure 5). The model is 90 m high in the *z*-direction, 80 m thick in the *y*-direction, and 30 m wide in the *x*-direction (Figure 5a).

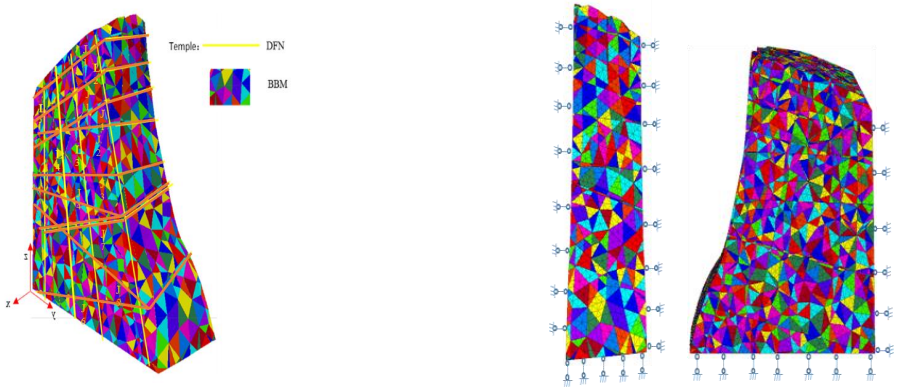

(**a**) (**b**)

Figure 5. High-steep scarp slope model on the left bank of the dam site of Huangzangsi Water Conservancy Project and boundary conditions. (**a**) Local model for the high-steep scarp slope. (**b**) Boundary conditions of the model of the high-steep scarp slope.

Since this article primarily focuses on the rockfall phenomenon on the high-steep scarp slope's overhanging face and the controlling effect of dominant joints on slope collapse, the model retains only the overhanging face and the top surface as free faces. At the same time, constraints are applied to four faces: the left, right, bottom, and back faces (Figure 5b).

3.4. Parameter Selection of the BBM–DFN Coupling Model for the High-Steep Scarp Slope

To reproduce a collapse of the high-steep scarp slope on the left bank of the dam site of the Huangzangsi Water Conservancy Project, rock samples were taken from the site and processed, followed by laboratory testing to obtain basic mechanical parameters of the rock samples. In tandem with the modified Bandis empirical formula proposed by Jin et al. [49], the parameters obtained in laboratory tests were converted into the parameters needed for simulation. These parameters were then compared with those obtained by Wu [50], Chen [51], and Wang [52], and with preliminary parameters provided by the construction team, thus determining parameters of the rock (Table 2).

Table 2. Parameters of rock masses in the BBM–DFN model for the high-steep scarp slope on the left bank of the dam site of the Huangzangsi Water Conservancy Project.

	Density/(kg/m^3)	Bulk Modulus/GPa	Shear Modulus/Gpa	Tensile Strength/Mpa	Internal Friction Angle/°	Cohesion/Mpa
Mechanical parameters of rock mass	2.69	2.7	1.14	8.6	35	4.53

By comparing the inversion results of numerical simulation with monitoring data recorded at the construction site, and referring to parameters recommended by the geological exploration report, parameters of mesoscopic joints between blocks in the BBM–DFN model for the high-steep scarp slope of interest were attained (Table 3).

Table 3. Parameters of mesoscopic joints between blocks in the BBM–DFN model for the high-steep scarp slope on the left bank of the dam site of the Huangzangsi Water Conservancy Project.

	Normal Stiffness/GPa	Shear Stiffness/GPa	Tensile Strength/MPa	Internal Friction Angle/°	Cohesion/MPa
Mechanical parameters for mesoscopic joints in BBM	56	30	5	20	2
Mechanical parameters for joints in DFN	56	30	0.09	20	0.21

Nine displacement monitoring points were arranged on the free face of the high-steep scarp slope based on the failure and convergence criteria proposed in Section 2.3, and the actual collapse locations during the engineering construction. The locations of the monitoring points are displayed in Figure 6. Based on the cumulative experience gained from step-by-step simulations, it is concluded that placing three monitoring points evenly at the top, middle, and bottom of the high-steep scarp slope's overhanging surface is sufficient to accurately capture the displacement patterns of the high-steep scarp slope's overhanging face.

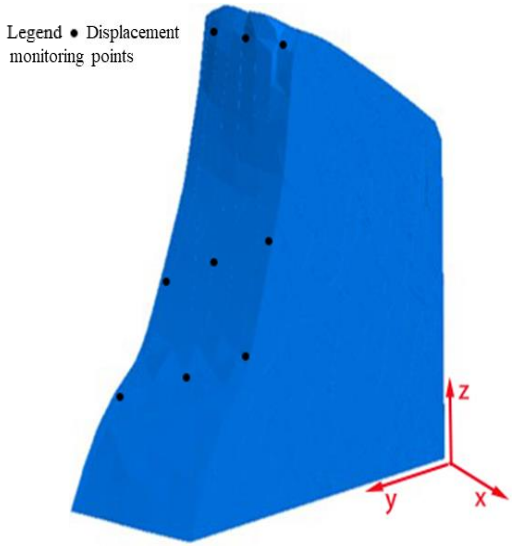

Figure 6. Distribution of monitoring points on the scarp model on the left bank of the dam site of the Huangzangsi Water Conservancy Project.

4. Stability Study of the High-Steep Scarp Slope on the Left Bank of Huangzang Temple Based on the BBM Planar Model

According to the reduction calculations, the safety factor for CF-RM is 2.57, the one for CFT-RM is 2.57, and the one for CFD-RM is 2.76. Figure 7a,b represent the high-steep scarp slope evolution curves for CF-RM and CFT-RM, respectively, with a reduction factor of 2.57. Figure 6c shows the steep cliff crack evolution curve for CFD-RM with a reduction factor of 2.76. Comparing the vertical axes, it is evident that the crack count under CFD-RM is significantly higher than that under CF-RM and CFT-RM when both are simulated for 40,000 steps. Comparing the positions of the curves leaving the horizontal axis in the three graphs, CFD-RM departs from the axis earliest, occurring between 5000 and 7500 steps. The one for CF-RM occurs at 7500 steps, and the one for CFT-RM occurs the latest, between 7500 and 10,000 steps.

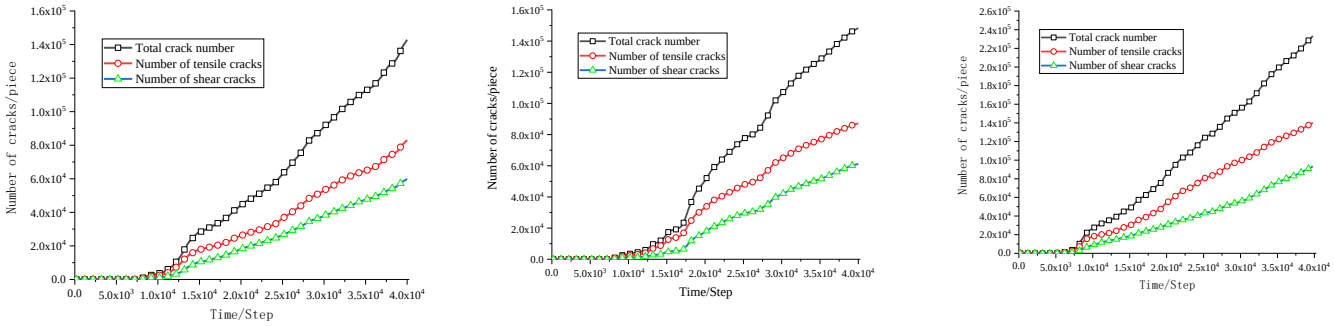

(**a**) (**b**) (**c**)

Figure 7. Variation trends in crack numbers under three different reduction methods. (**a**) Reduction curves of the scarp slope in the CF-RM process. (**b**) Reduction curves of the scarp slope in the CFT-RM process. (**c**) Reduction curves of the scarp slope in the CFD-RM process.

A comparison of the high-steep scarp slope failure cloud patterns under the three reduction methods was conducted at four specific time points: the initiation of crack development, the appearance of transverse cracks, transverse crack propagation, and finally longitudinal crack propagation, as shown in Figures 8–13.

Figures 8–13 provide a comparative analysis of crack distribution and block velocity at four time points; namely, from the initiation of cracks to the appearance of transverse cracks, then transverse crack propagation, and finally longitudinal crack propagation leading to complete slope failure, under three different reduction methods.

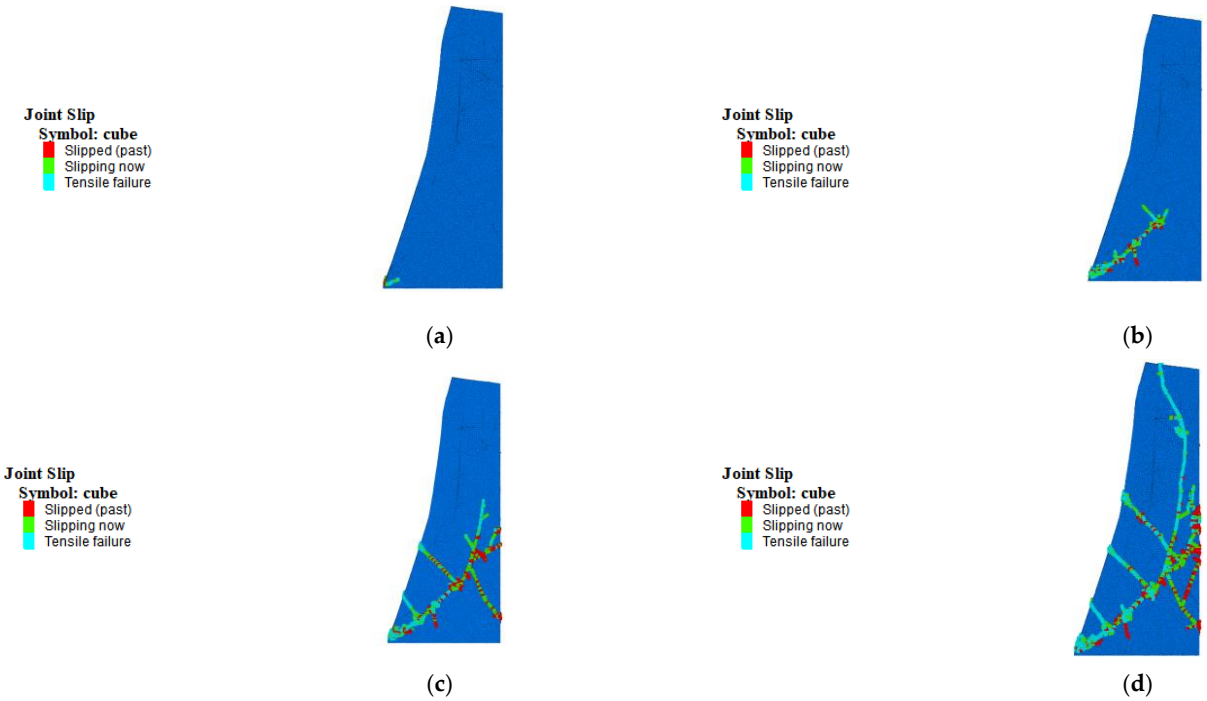

(**a**) (**b**)

(**c**) (**d**)

Figure 8. Distribution of cracks in the high-steep scarp slope in the CFD-RM reduction method. (**a**) The initiation of crack development (5000 steps). (**b**) The appearance of transverse cracks (8000 steps). (**c**) Transverse crack propagation (10,000 steps). (**d**) Finally, longitudinal crack propagation (13,000 steps).

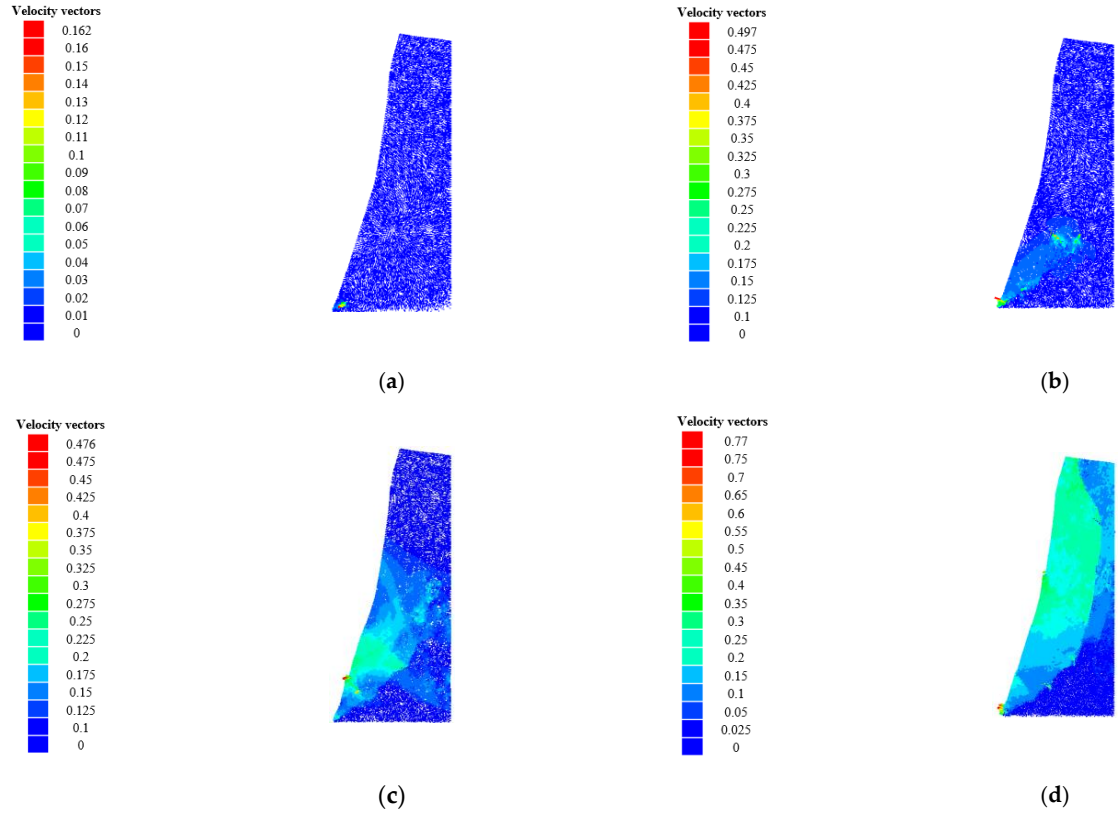

Figure 9. Block velocity(m/s) of the high-steep scarp slope in the CFD-RM reduction method. (**a**) The initiation of crack development (5000 steps). (**b**) The appearance of transverse cracks (8000 steps). (**c**) Transverse crack propagation (10,000 steps). (**d**) Finally, longitudinal crack propagation (13,000 steps).

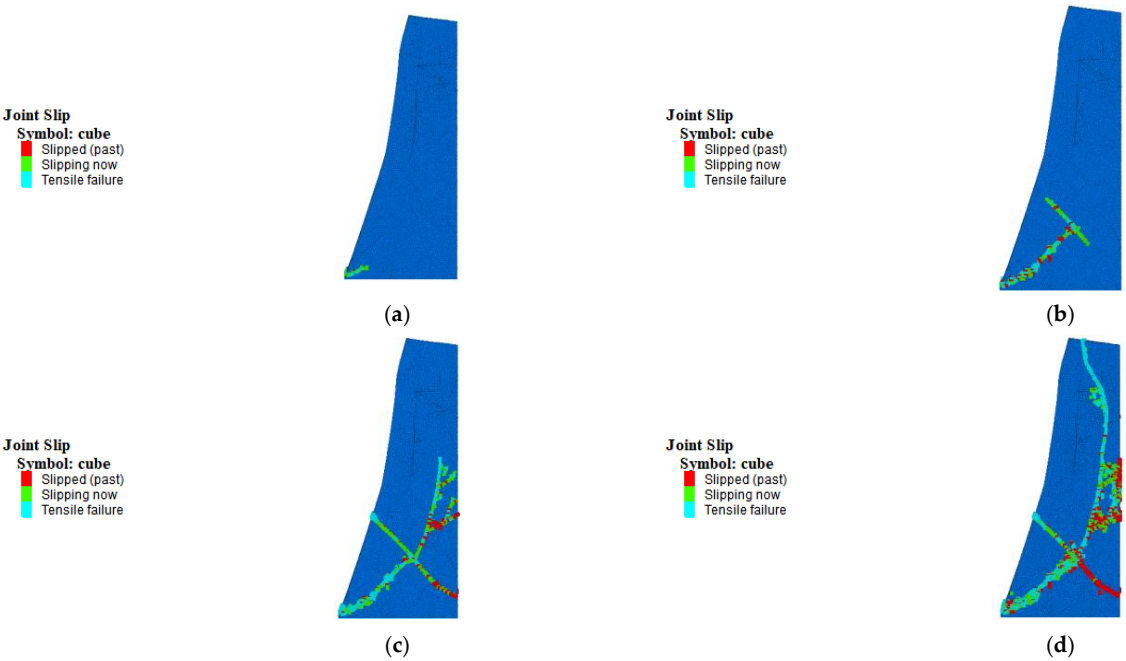

Figure 10. Distribution of cracks in the high-steep scarp slope in the CF-RM reduction method. (**a**) The initiation of crack development (8000 steps). (**b**) The appearance of transverse cracks (12,000 steps). (**c**) Transverse crack propagation (14,000 steps). (**d**) Finally, longitudinal crack propagation (20,000 steps).

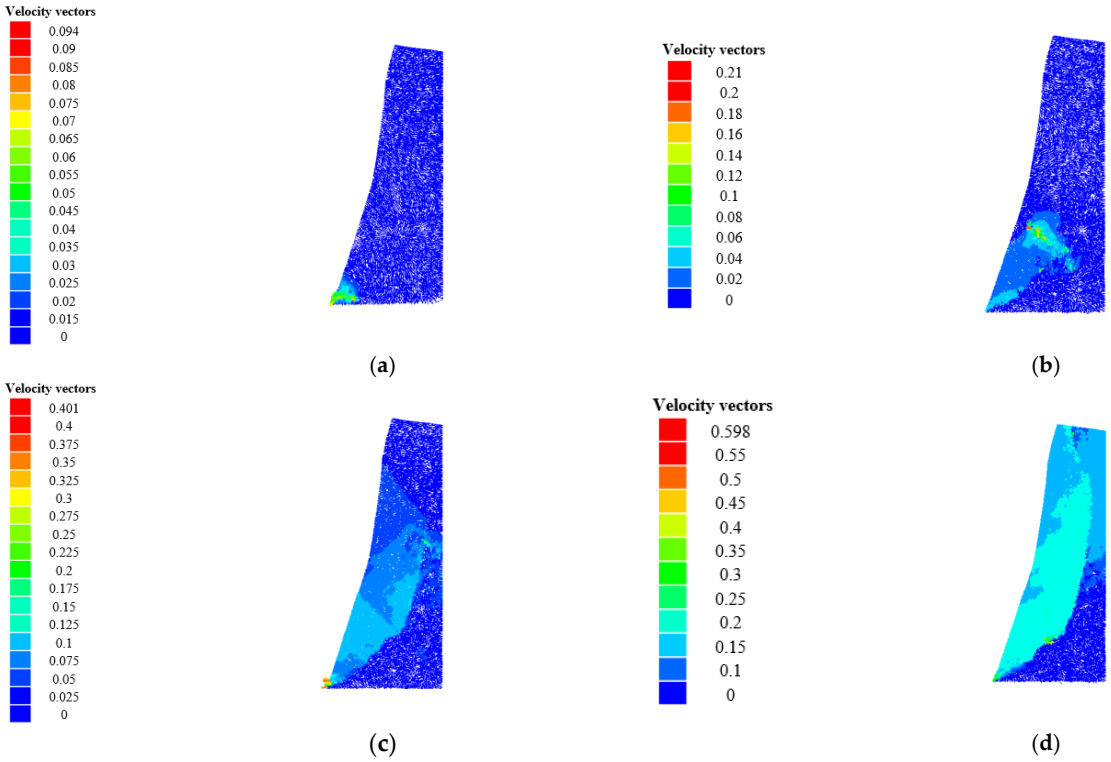

Figure 11. Block velocity(m/s) of the high-steep scarp slope in the CF-RM reduction method. (**a**) The initiation of crack development (8000 steps). (**b**) The appearance of transverse cracks (12,000 steps). (**c**) Transverse crack propagation (14,000 steps). (**d**) Finally, longitudinal crack propagation (20,000 steps).

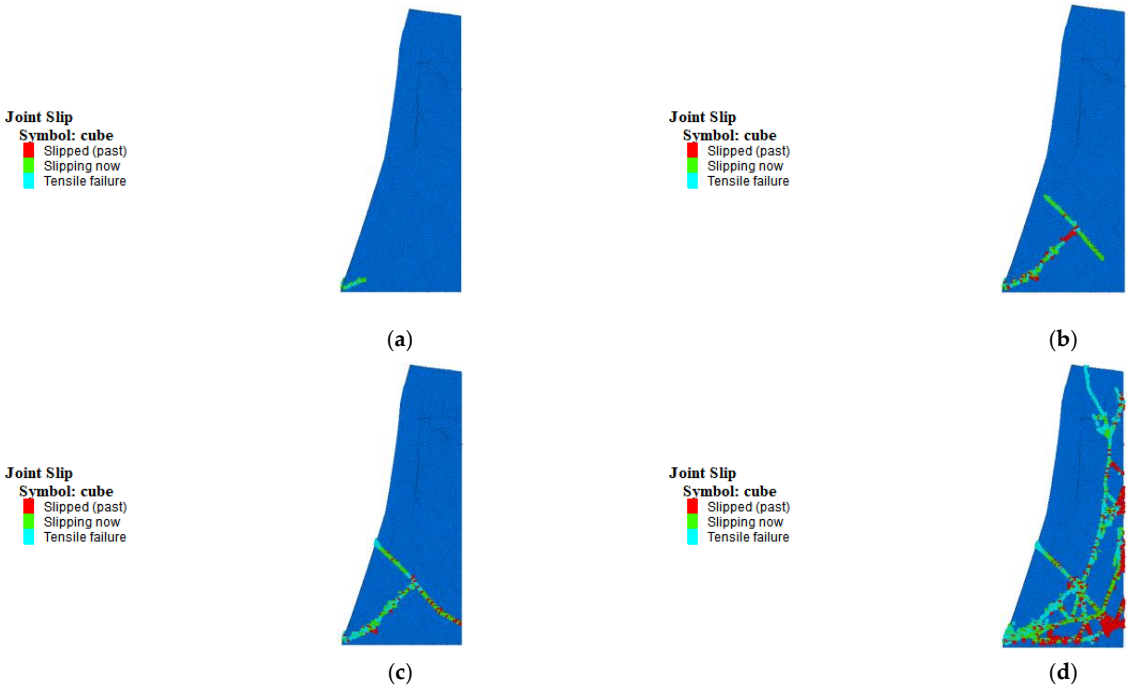

Figure 12. Distribution of cracks in the high-steep scarp slope in the CFT-RM reduction method. (**a**) The initiation of crack development (8000 steps). (**b**) The appearance of transverse cracks (13,000 steps). (**c**) Transverse crack propagation (14,000 steps). (**d**) Finally, longitudinal crack propagation (23,000 steps).

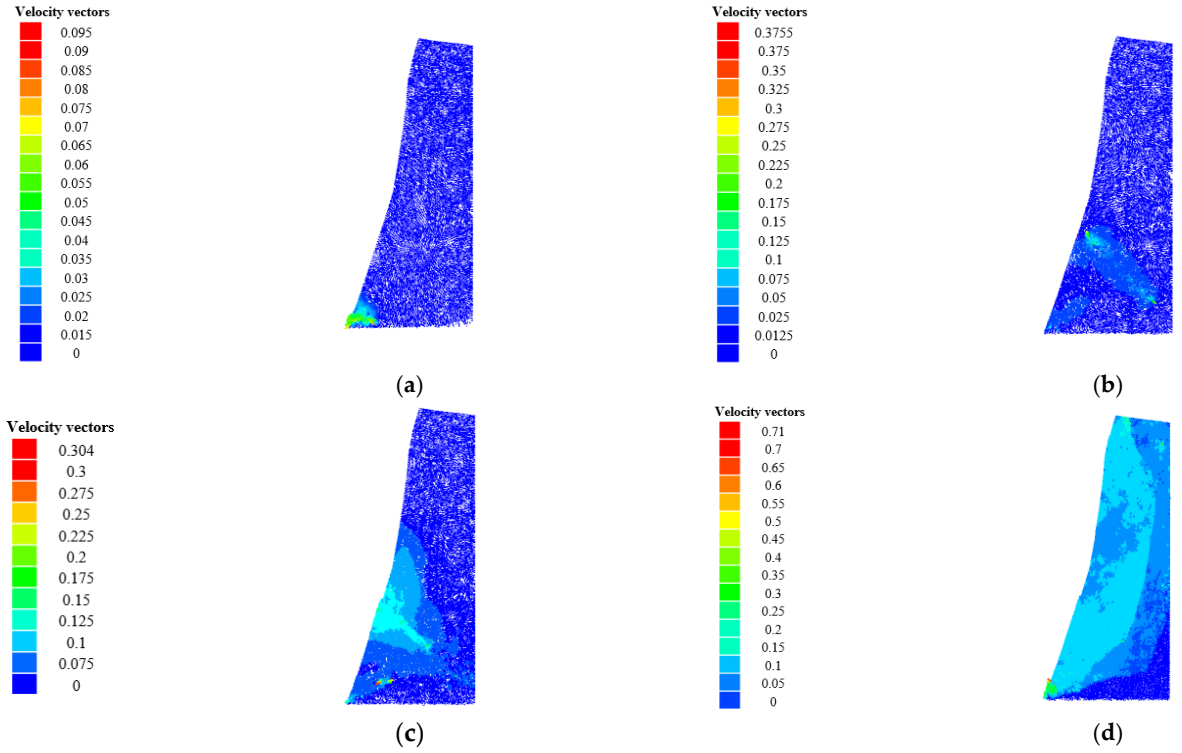

Figure 13. Block velocity(m/s) of the high-steep scarp slope in the CFT-RM reduction method. (**a**) The initiation of crack development (8000 steps). (**b**) The appearance of transverse cracks (13,000 steps). (**c**) Transverse crack propagation (14,000 steps). (**d**) Finally, longitudinal crack propagation (23,000 steps).

In Figures 8 and 9, it can be observed that under the CFD-RM reduction method, cracks initiate from the lower left corner of the model and propagate upwards along the slope angle bisector. At 8000 steps, signs of transverse crack extension become apparent, and simultaneously, there is evidence of rockfall at the base of the slope, with a velocity of 0.5 m/s. At 10,000 steps, transverse cracks fully propagate, evenly distributed on both sides of the main longitudinal crack as it develops. Block fall occurs at the high-steep scarp slope overhang where cracks propagate, with a velocity of 0.475 m/s. Finally, at 13,000 steps, longitudinal cracks propagate completely, resulting in the complete failure of the steep cliff. There are three locations on the overhang where transverse cracks penetrate, leading to block fall both at the crack locations and the base of the slope, with velocities ranging from 0.5 m/s to 0.77 m/s.

Figures 10 and 11 show that under the CF-RM reduction method, crack initiation occurs at the same position, in the lower left corner of the model, and propagates upwards along the angle bisector. At 12,000 steps, signs of transverse crack extension appear, and after 14,000 steps, transverse cracks fully propagate, with only one transverse crack. Block ejection occurs at the base of the steep cliff with a velocity of 0.4 m/s. At 20,000 steps, the main longitudinal crack propagates completely, with transverse cracks penetrating except at the rear edge of the high-steep scarp slope, where they are more densely distributed.

Figures 12 and 13 indicate that under the CFT-RM reduction method, the early crack development trend is similar to that under the CF-RM reduction method. However, there is no block ejection at the base of the high-steep scarp slope until the transverse cracks fully propagate. Additionally, the maximum velocity point is located below the main longitudinal crack. As the reduction process progresses, at 23,000 steps, longitudinal cracks propagate, creating a ripple-like pattern of cracks expanding from the main longitudinal crack towards the rear edge. Shorter cracks connect between the ripple crests, and block ejection occurs approximately five meters above the slope angle.

5. Factors Influencing the Stability of the High-Steep Scarp Slope Based on the BBM–DFN Model

5.1. Coupling Effects of the Internal Friction Angle and Cohesion of Mesoscopic Joints between Blocks in the BBM–DFN Model on the Stability of the High-Steep Scarp

It can be seen from Figure 14a that the numerical simulation of the high-steep scarp fails to converge, and the curves for the number of cracks and for average displacement at monitoring points ascend abruptly if the reduction coefficient reaches 2.25, so the safety factor for CF-RM is set to 2.24. As shown in Figure 14c, tensile cracks are dominant when the reduction starts; then, shear cracks gradually increase in number and become dominant as the reduction coefficient grows, while the number of tensile cracks does not change to any significant extent. As shown in Figure 14e, cracks are mainly shear cracks distributed mainly at dominant joints inside the high-steep scarp before failure. Figure 14b shows that, if the reduction coefficient for the high-steep scarp is less than 2.1, the CV curves are similar; once the reduction coefficient exceeds 2.3, the curves fluctuate more greatly at the beginning and stabilize after 70,000 to 100,000 steps in the simulation, which means that the scarp slope has been damaged and the simulation converges between these steps. Therefore, results corresponding to 90,000 steps and a reduction coefficient of 2.25 were selected to investigate collapse failure of the scarp slope. As shown in Figure 14d, tensile cracks are dominant at the beginning of computation, and there are more shear cracks than tensile cracks between 2000 to 10,000 steps—the time period during which the total number of cracks increases most quickly. Figure 14f shows that blocks on the top of the scarp slope and overall rock connection in the rear of the slope are heavily damaged. Taken together, the coupling analysis of the internal friction angle and cohesion of mesoscopic joints between blocks indicates that failure of the scarp slope is mainly manifest as fracture of rock bridges due to decreased bonding parameters at the four dominant joints, and failing of several rock blocks from the free face on the top of the scarp slope is due to decreased cohesion between rock blocks.

5.2. Coupling Effects of the Internal Friction Angle, Cohesion, and Tensile Strength of Mesoscopic Joints between Blocks in the BBM–DFN Model on the Stability of the High-Steep Scarp

As illustrated in Figure 15a, the simulation fails to converge, and the curves of the number of cracks and average vertical displacement show abrupt changes when the reduction coefficient is 1.86, so the safety factor of the scarp slope is set to 1.85 in the CFT-RM. Figure 15c shows that tensile cracks are always dominant in the reduction process, and their increase shows a trend similar to that of the total number of cracks, while the number of shear cracks increases slowly. Figure 15e shows the presence of points indicating tensile cracks on the top surface of the rock mass, suggesting that the scarp slope is subject to potential rockfall risks before the key parameters reach their critical thresholds. Figure 15b shows that the CV curves are similar when the reduction coefficient is less than 1.7, and the curves fluctuate more remarkably when the reduction coefficient is greater than 1.9. In addition, the curves tend to be stable when the simulation has run to between 40,000 and 100,000 steps, which indicates that the scarp slope has been damaged, and the simulation converges during these steps. Therefore, results corresponding to a reduction coefficient of 1.85 and 90,000 steps are taken to discuss the fracture of the scarp slope. It can be seen from the change curves of the number of cracks during the calculation of critical parameters in Figure 15d that the proportion of shear cracks abruptly increases in the initial failure period, while the number does not exceed that of tensile cracks. As the failure mode gradually stabilizes, the dominance of tensile cracks becomes more definite. As can be seen from Figure 15f, not only does fracture occur at joints in the DFN, but much damage and multiple cracks are observed on the free face of the scarp slope. Collectively, in the analysis of coupling of the internal friction angle, cohesion, and tensile strength of mesoscopic joints between blocks, the fracture of rock bridges occurs at the four dominant joints and intersections between multiple dominant joints with the reduction of the parameters. At the same time, the decrease in cohesion between intact rock also induces falling of many rock blocks from the top of the scarp slope.

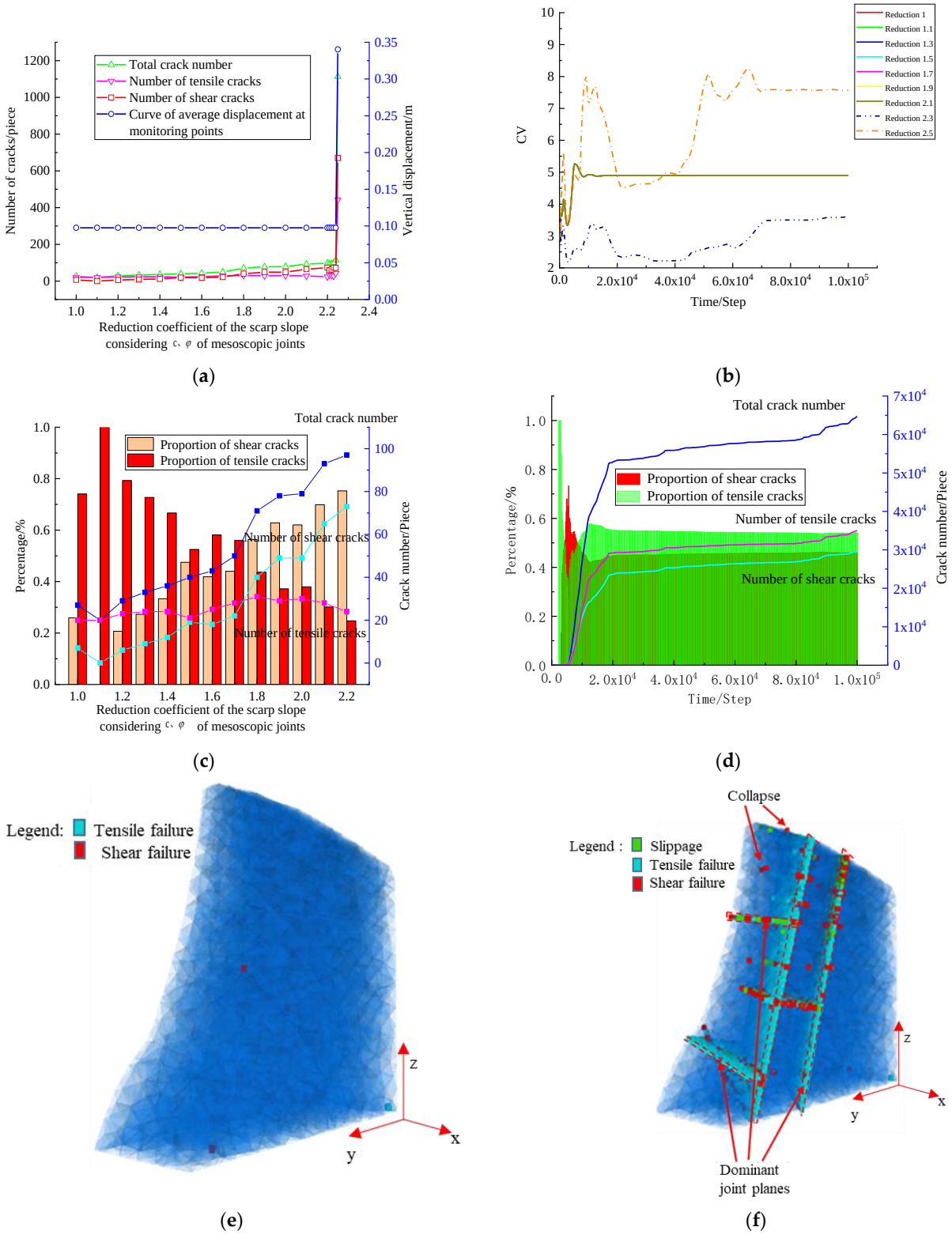

Figure 14. Coupling effects of the internal friction angle and cohesion of mesoscopic joints between blocks on the stability of the scarp slope. (**a**) Reduction curves of the scarp slope in the CF-RM process. (**b**) Changes of the CV in the CF-RM process. (**c**) Changes in the number of cracks in the scarp slope in the CF-RM process. (**d**) Changes in the number of cracks during failure in the CF-RM process. (**e**) Distribution of cracks in the scarp slope before failure in the CF-RM process. (**f**) Distribution of cracks in the scarp slope at failure in the CF-RM process.

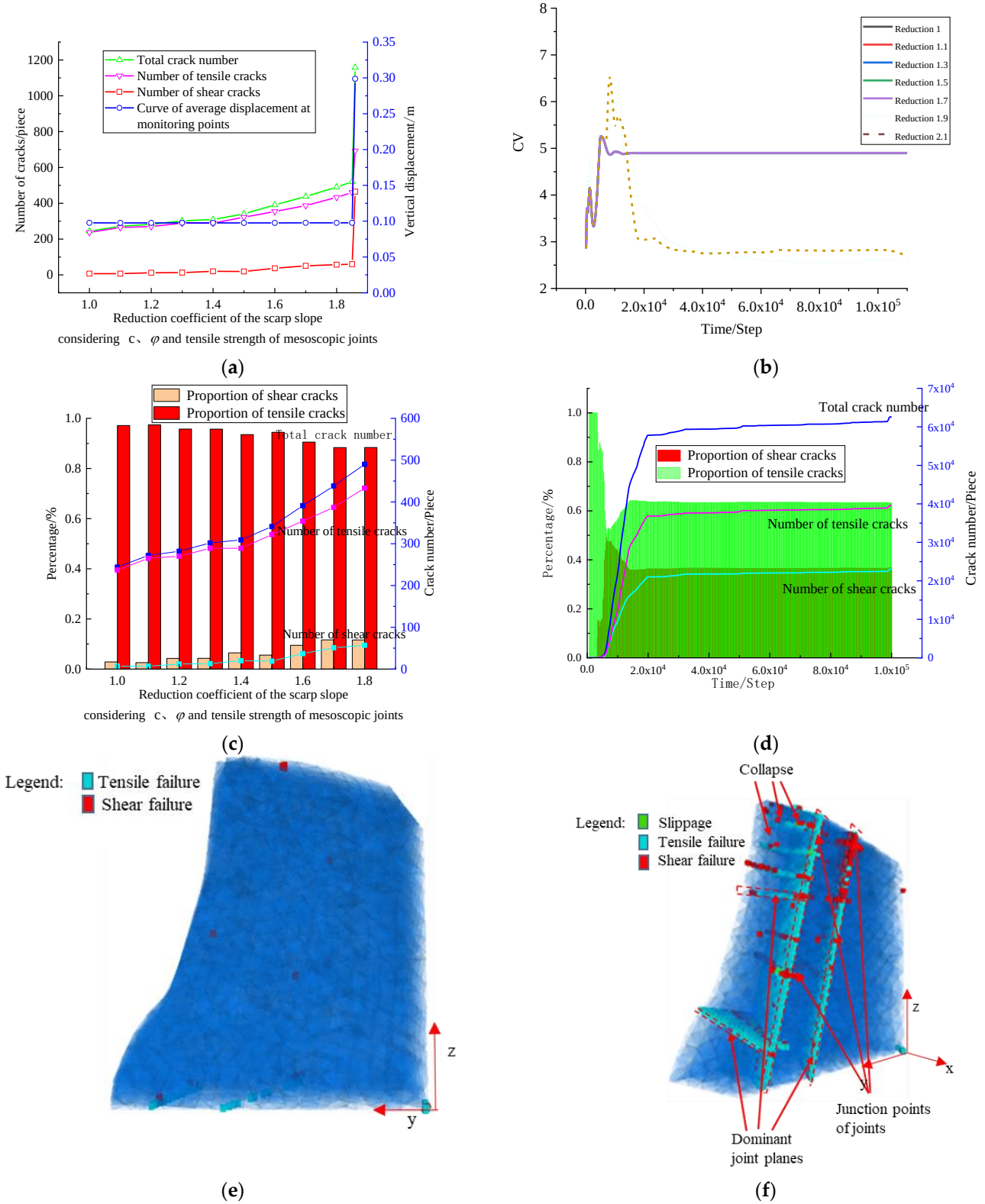

Figure 15. Coupling effects of the internal friction angle, cohesion, and tensile strength of mesoscopic joints between blocks on the stability of the scarp slope. (**a**) Reduction curves of the scarp slope in the CFT-RM process. (**b**) Changes of the CV in the CFT-RM process. (**c**) Changes in the number of cracks in the scarp slope in the CFT-RM process. (**d**) Changes in the number of cracks during failure in the CFT-RM process. (**e**) Distribution of cracks in the scarp slope before failure in the CFT-RM process. (**f**) Distribution of cracks in the scarp slope at failure in the CFT-RM process.

5.3. Coupling Effects of the Internal Friction Angle, Cohesion, and Deformation Parameters of Mesoscopic Joints between Blocks in the BBM–DFN Model on the Stability of the High-Steep Scarp Slope

It can be seen from Figure 16a that when the reduction coefficient is 2.04, the simulation fails to converge, and abrupt changes occur in the curves showing the number of cracks and average vertical displacement, so the safety factor in the CFD-RM is determined to be 2.03. The reduction results of the deformation parameters in Figure 16c reveal that tensile cracks are dominant at the beginning of reduction, while the shear cracks gradually account for a larger proportion in the reduction process; their number finally exceeds that of tensile cracks at the brink of failure. Figure 16e reveals that cracks only occur within the rock mass before failure. As shown in Figure 16b, the CV curves are similar when the reduction coefficient is less than 1.9; the curves fluctuate more significantly and gradually stabilize during simulation for 100,000 to 140,000 steps when the reduction coefficient increases to 2.1. This indicates that the scarp slope has been damaged and the simulation converges between these steps, so results corresponding to a reduction coefficient of 2.04 and 100,000 steps are chosen to analyze the fracture in the slope. It can be seen from Figure 16d that tensile cracks are dominant most of the time, while the number of shear cracks exceeds that of tensile cracks only in the initial period when it grows rapidly. Figure 16f shows that cracks are mainly present on both sides of the longitudinal dominant joints. In summary, rock bridges are only fractured on the two longitudinal dominant joint planes, and only a few rock blocks fall off from the free face when the parameters reduce in the analysis of coupling of the internal friction angle, cohesion, and deformation parameters of mesoscopic joints.

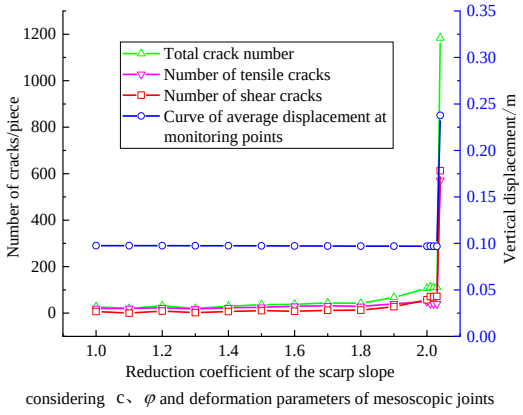

(**a**)

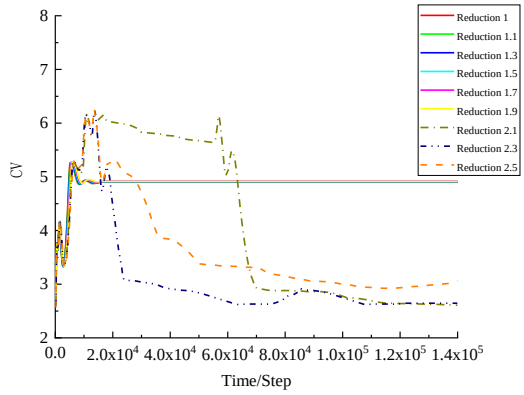

(**b**)

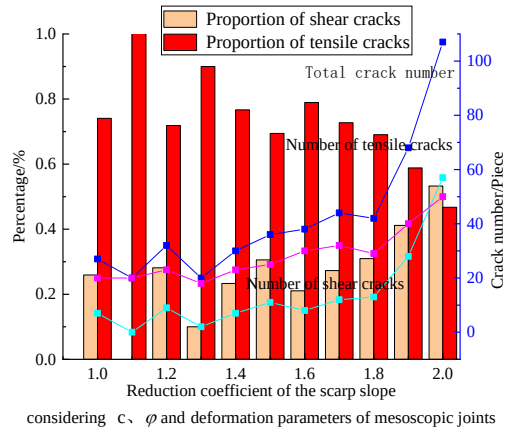

(**c**)

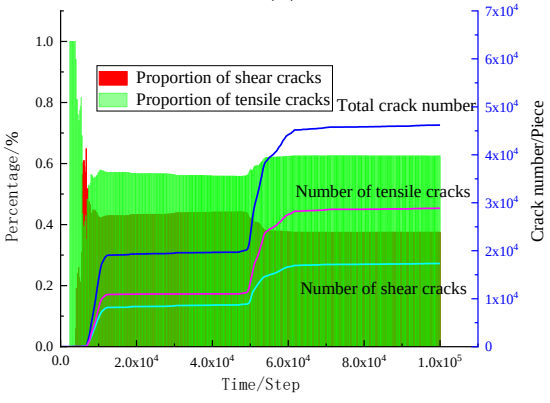

(**d**)

Figure 16. *Cont.*

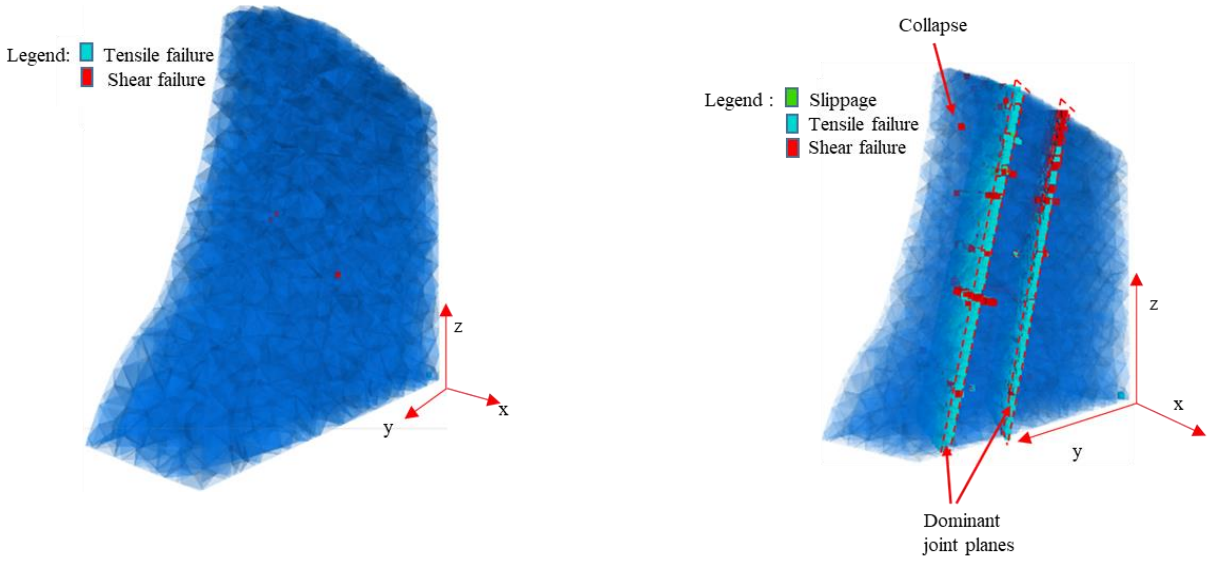

Figure 16. Coupling effects of the internal friction angle, cohesion, and deformation parameters of mesoscopic joints between blocks on the stability of the scarp slope. (**a**) Reduction curves of the scarp slope in the CFD-RM process. (**b**) Changes of the CV in the CFD-RM process. (**c**) Changes in the number of cracks in the scarp slope in the CFD-RM process. (**d**) Changes in the number of cracks during failure in the CFD-RM process. (**e**) Distribution of cracks in the scarp slope before failure in the CFD-RM process. (**f**) Distribution of cracks in the scarp slope at failure in the CFD-RM process.

6. Discussion

In Section 5, it was found that when only the central part of the high-steep scarp slopes is simulated, damage zones appear at the boundaries of the high-steep scarp slopes. The question of whether this phenomenon affects the authenticity of the simulation is in need of urgent discussion. Therefore, based on these issues, we have developed a new model, as shown in Figure 17a. This model is based on the actual high-steep scarp slopes, with the middle portion representing the simulated section in the article. Finite element models are established on both sides of this simulated portion, and the rock parameters are listed in Table 2. We subjected this model to CF-RM reduction and compared its results to those in the article, as shown in the comparative graph in Figure 18.

From Figure 18a,b, it can be observed that when both sides are intact rock masses, the damage and settlement are primarily concentrated in the central portion. Therefore, for the subsequent analysis, only the central portion is selected for analysis. Comparing Figure 18c,d, it is evident that the failure modes of the model in both cases involve joint surface failure and overhanging rock collapse. Additionally, it can be observed that in the new model, substantial damage occurs at the interface between the BBM-DFN model and the intact rock mass, consistent with the results of the model presented in the article. Comparing Figure 18e,f, it is evident that the safety factors of the two models are close, measuring 2.22 and 2.24, respectively. The crack growth patterns in both models are similar, with a significant increase occurring just prior to failure.

In conclusion, it can be seen that, due to the relatively low joint surface parameters, both the complete model and the local model produce damage zones at the boundaries of the BBM-DFN model. The safety factors of the two models are similar, and the growth pattern of joint cracks is the same. Therefore, the boundary conditions used in this study are equivalent to the boundary conditions when both sides are considered as complete rock masses.

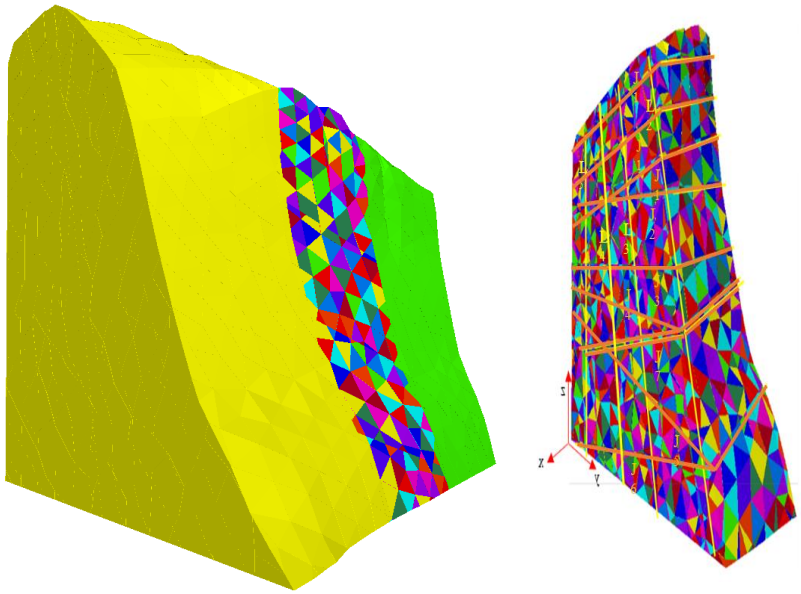

(**a**) (**b**)

Figure 17. High-steep scarp slope model on the left bank of the dam site of the Huangzangsi Water Conservancy Project and boundary conditions. (**a**) The complete model. (**b**) The model in the article.

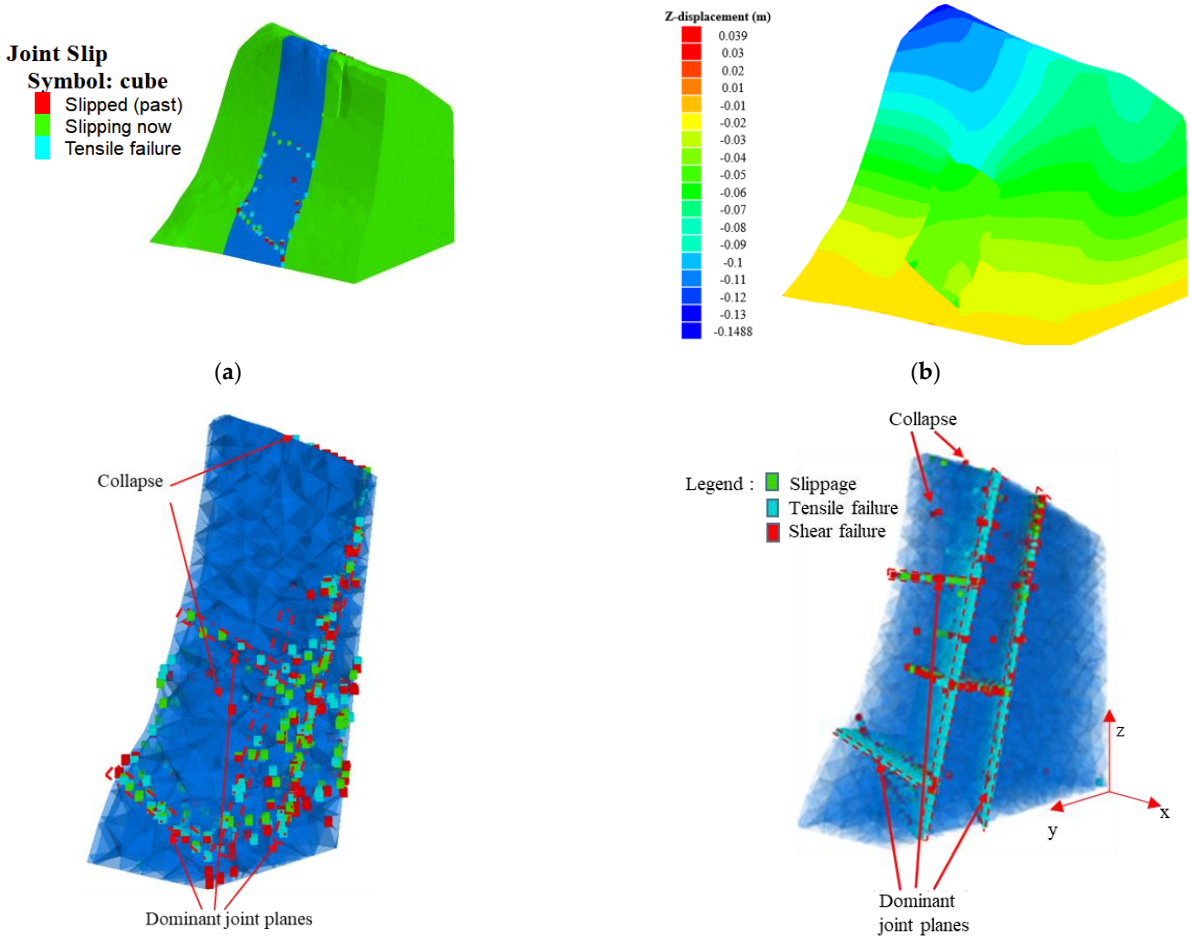

(**a**) (**b**)

(**c**) (**d**)

Figure 18. *Cont.*

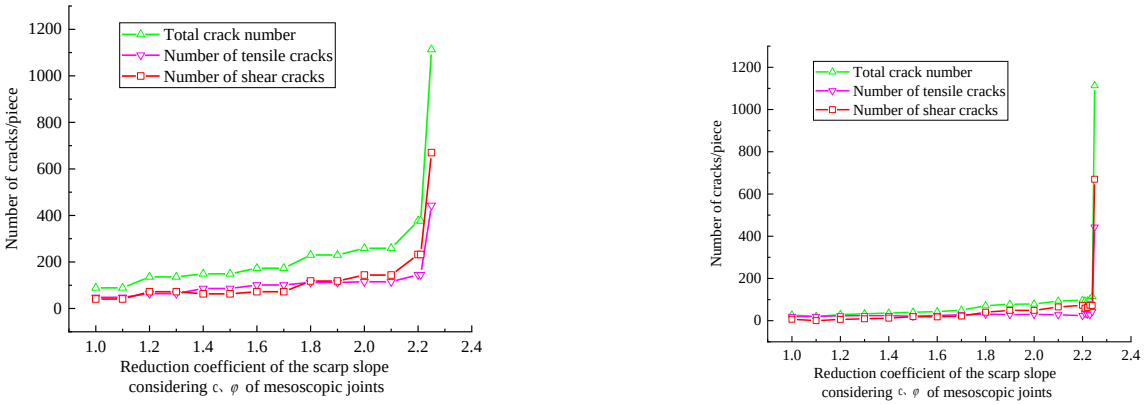

(**e**) (**f**)

Figure 18. Comparison of computational results between the new model and the model presented in the article. (**a**) The complete model diagram when it is disrupted. (**b**) Z-displacement of the model when it is disrupted. (**c**) Distribution of cracks in the scarp slope at failure in the new model. (**d**) Distribution of cracks in the scarp slope at failure in the article. (**e**) Reduction curves of the scarp slope in the new model. (**f**) Reduction curves of the scarp slope in the article.

The primary focus of this article is on the mechanism of rockfall in the high-steep scarp slopes near the central free face, so the influence of boundary conditions is relatively minor. The model currently chosen is a compromise solution determined by considering an adequate number of discrete blocks to properly represent the instability mechanism of the steep cliff and the computational capabilities of three-dimensional block elements. One limitation of using the BBM-DFN method is that the number of discrete block elements cannot be excessive, as this would result in a significant increase in computational time.

7. Conclusions

Due to the potential risk of high-steep scarp slopes and the complexity of the natural geometry of such slopes, structural features of rock mass, and mechanisms of occurrence of collapse, a coupled BBM–DFN model has been established. Based on this model, fracture behaviors of intact rock and rock bridges during collapse were discussed. The calculation methods for the optimal safety factor were determined, and factors influencing its collapse were analyzed. In this way, the following conclusions are drawn:

(1) In view of the collapse and failure situation of high-steep scarp slopes and the nature of the coupled BBM–DFN model, comprehensive consideration of abrupt changes in displacement at monitoring points, abrupt ascent of curves of the number of cracks, and non-convergence of numerical simulation are taken as the collapse criteria. In addition, the gradual flattening of the CV curve for displacement at monitoring points to the horizontal direction as the discriminant for convergence of calculation.

(2) In the CF-RM, failure of the high-steep scarp slope mainly entails fracture of rock bridges at the four dominant joints due to a decrease in bonding parameters and falling of several rock blocks from the free face on the top of the slope because of the decreased cohesion of the rock. In the CFT-RM, rock bridges are mainly fractured at the four dominant joints and at the intersection of multiple dominant joints. At the same time, many rock blocks on the top of the scarp slope fall due to the decreased cohesion between them and the intact rock. In the CFD-RM, fracture of rock bridges is only seen on two longitudinal dominant joint planes, and only a few rock blocks fall from the free face. Construction at dominant joints, especially at the intersection of dominant joints, should be paid heed.

(3) In the CF-RM, CFT-RM, and CFD-RM, the safety is 2.24, 1.85, and 2.03, respectively. After comparing the three aforementioned reduction methods, the safety factor of the high-steep scarp slope is set to 1.85 for the sake of safety. Considering the fracture

behaviors in the CFT-RM, displacement monitoring devices should be installed, and collapse-prevention measures should be implemented at the top of the scarp slope to ensure safety of construction.

Author Contributions: Conceptualization, Z.S., S.Q. and Z.W.; methodology, Z.S. and S.Q.; software, Z.S.; validation, Z.S., S.Q. and Z.W.; formal analysis, Z.S.; data curation, S.Y.; writing—original draft preparation, Z.S.; writing—review and editing, Z.S., S.Q. and Z.W; supervision, S.Q, S.Y. and Z.W; project funding acquisition, S.Q. All authors have read and agreed to the published version of the manuscript.

Funding: The work was supported by the National Natural Science Foundation of China (Grant Nos 41877256 and 51879261) and the Joint Funds of the National Natural Science Foundation of China (Grant No. U1965205).

Institutional Review Board Statement: Not applicable.

Informed Consent Statement: Not applicable.

Data Availability Statement: Data is contained within the article. The data presented in this study are available in Tables 1–3 and Figures 7, 14–16 and 18.

Conflicts of Interest: The authors declare no conflict of interest.

References

1. Cheng, Q.; Zhang, Z.; Huang, R. Research status and development trend of high−speed and long−range avalanche dynamics. *Mt. Res.* **2007**, *1*, 72–84.
2. Li, X.; Xie, Q.; Liu, X. *Technical Report on Investigation of "7.13" Dangerous Rock Collapse Accident in Hekou Granite Mine of Cenxi Tianma Stone Co., Ltd.*; Tianma Stone Industry Co., Ltd.: Cenxi, China, 2019.
3. Wang, Z.; Yan, E.; Liu, J.; Ren, B. Failure characteristics and formation mechanism analysis of reverse dip rock slope in Honglianchi iron mine, Hefeng, Hubei Province. *Chin. J. Geol. Hazard Control.* **2016**, *27*, 7–13.
4. Li, Y.; Tan, K.; Wang, X. Characteristics and Genesis of Jiguanling Rock Collapse in Wujiang River. *Geol. China* **1994**, *7*, 25–27.
5. Yin, Y.; Liu, C.; Chen, H.; Ren, J.; Zhu, C. Study on the catastrophic landslide in Zhaojiagou, Zhenxiong, Yunnan on 11 January 2013. *J. Eng. Geol.* **2013**, *21*, 6–15.
6. Sun, Y.; Yao, B. Study on the mechanism of mountain collapse in Yanchihe phosphate mine. *Hydrogeol. Eng. Geol.* **1983**, *1*, 1–7.
7. Liu, C.Z.; Guo, Q.; Chen, H.Q. Preliminary analysis on the causes of dangerous rock collapse in Yanjiaozhai, Nayong County, Guizhou Province. *Chin. J. Geol. Hazard Control.* **2004**, *15*, 123+144.
8. Fang, C.; Wang, J.; Li, Y.; Jia, M. Research on Numerical Simulation of Natural Caving Method Based on PFC2D−DFN. *Gold Sci. Technol.* **2019**, *27*, 189–198.
9. Bolla, A.; Paronuzzi, P. Numerical Investigation of the Pre-collapse Behavior and Internal Damage of an Unstable Rock Slope. *Rock Mech. Rock Eng.* **2019**, *53*, 2279–2300. [CrossRef]
10. Cui, F.P.; Hu, R.L.; Yin, Y.P.; Xu, Q.; Zhang, M. Discrete element analysis of collapsing and sliding response of slope triggered by time difference coupling effects of pands seismic waves—Taking tangjiashan landslide in beichuan county for example. *Chin. J. Rock Mech. Eng.* **2010**, *29*, 319–327.
11. Chen, M.; Lu, W.; Yan, P.; Zhou, C. New method for dynamic stability analysis of rock slope under blasting vibration based on equivalent acceleration and Sarma method. *Can. Geotech. J.* **2013**, *51*, 441–448. [CrossRef]
12. Borrelli, L.; Greco, R.; Gullà, G. Weathering grade of rock masses as a predisposing factor to slope instabilities: Reconnaissance and control procedures. *Geomorphology* **2006**, *87*, 158–175. [CrossRef]
13. Xu, J.; Li, K.; Chen, P.; Liu, Y. Simulation of rockfall at Mingshan in Fengdu by discrete element method. *Rock Soil Mech.* **2004**, *11*, 1819–1822.
14. Oliveira, S.N.; Filho RC, O.; Marton, E.; Silva, C. Correlation between rainfall and landslides in Nova Friburgo, Rio de Janeiro-Brazil: A case study. *Environ. Earth Sci.* **2016**, *75*, 1358. [CrossRef]
15. Ha, N.D.; Satoshi, G.; Shinro, A.; Miyagi, T.; Hayashi, K.; Watanabe, O. Torrent rainfall-induced large-scale karst limestone slope collapse at Khanh waterfall, Hoa Binh Province, Vietnam. *Geoenviron. Disasters* **2022**, *9*, 4.
16. Griffiths, D.V.; Lane, P.A. Slope stability analysis by finite element. *Geotechnique* **1999**, *49*, 387–403. [CrossRef]
17. Morteza, N.; Hussein, G.; Danial, G.; Javanmardi, Y. Explicit finite element analysis of slope stability by strength reduction. *Geomech. Eng.* **2021**, *26*, 133–146.
18. Wang, D.; Nian, Y.; Chen, Y. Three problems in slope stability analyses with finite element method. *Rock Soil Mech.* **2007**, *11*, 2309–2313+2318.
19. Zhao, S.; Zheng, Y.; Zhang, Y. Study on slope failure criterion in strength reduction finite element method. *Rock Soil Mech.* **2005**, *2*, 332–336.

20. Manzari, M.; Tour, M.A. Significance of soil dilatancy in slope stability analysis. *J. Geotech. Geoenviron. Eng.* **2000**, *126*, 75–80. [CrossRef]
21. Luan, M.; Wu, Y.; Nian, Y. Plastic zone criterion of slope instability in strength reduction finite element method and its application. *J. Disaster Prev. Mitig. Eng.* **2003**, *03*, 1–8.
22. Acharya, M.; Timalsina, A.; Paudel, U. Shear Strength Reduction Analysis of Slope by Numerical Modelling Based on Finite Element Method. *Am. J. Sci. Eng. Technol.* **2023**, *8*, 125–132. [CrossRef]
23. Bai, Y.; Huang, R.; Ju, N.; Zhao, J.; Huo, Y. 3DEC stability analysis of high and steep rock slope. *J. Eng. Geol.* **2008**, *16*, 592–597.
24. Wang, T.; Sheng, Q.; Xiong, J. Research on numerical simulation of natural caving method based on particle flow method. *Chin. J. Rock Mech. Eng.* **2007**, *26*, 4202–4207.
25. Luirei, K.; Mehta, M.; Iqpal, A.; Nazir, S.; Kothyari, G.C. Factors influencing the slope instability of the Mussoorie-Bhitarli area, Garhwal Himalaya. *Geosci. J.* **2023**, *27*, 337–350. [CrossRef]
26. Bi, Y.; He, S.; Du, Y.; Sun, X.; Li, X. Effects of the configuration of a baffle–avalanche wall system on rock avalanches in Tibet Zhangmu: Discrete element analysis. *Bull. Eng. Geol. Environ.* **2019**, *78*, 2267–2282. [CrossRef]
27. Salavati, M.; Hosseinitoudeshki, V.; Gheidari, N.H.M. Stability Evaluation of High-steep Rock Slope by Microseismic. *J. Prog. Civ. Eng.* **2020**, *218*, 22–38.
28. Marie, H.S. Study on the influence of slope height and angle on the factor of safety and shape of failure of slopes based on strength reduction method of analysis. *Beni-Suef Univ. J. Basic Appl. Sci.* **2021**, *10*, 31.
29. Zhang, L.; Cong, Y.; Meng, F.; Wang, Z.; Zhang, P.; Gao, S. Energy evolution analysis and failure criteria for rock under different stress paths. *Acta Geotech.* **2021**, *16*, 569–580. [CrossRef]
30. Zhang, L.; Zhang, D.; Wang, Z.; Cong, Y.; Wang, X. Constructing a three-dimensional creep model for rocks and soils based on memory-dependent derivatives: A theoretical and experimental study. *Comput. Geotech.* **2023**, *159*, 105366. [CrossRef]
31. Zhang, L.; Chao, W.; Liu, Z.; Cong, Y.; Wang, Z. Crack propagation characteristics during progressive failure of circular tunnels and the early warning thereof based on multi-sensor data fusion. *Geomech. Geophys. Geo-Energy Geo-Resour.* **2022**, *8*, 172. [CrossRef]
32. Liming, Z.; Xiaoshan, W.; Yu, C.; Wang, Z.; Liu, J. Transfer mechanism and criteria for static–dynamic failure of granite under true triaxial unloading test. *Geomech. Geophys. Geo-Energy Geo-Resour.* **2023**, *9*, 104.
33. Xu, P.Y.; Zhang, L.M.; Zhang, J.Y.; Wang, J.X.; Zhang, S.L.; Zhang, P.C. Progressive failure characteristics and failure symptoms of straight-walled arched sandstone tunnels. *Acadlore Trans. Geosci.* **2023**, *2*, 46–57. [CrossRef]
34. Hongjian, L.; Pan, W. Stability analysis of gentle dip thick ore body mining based on the integration of SURPAC-FLAC3D. *Acadlore Trans. Geosci.* **2023**, *2*, 58–69.
35. Chen, M.; Zhang, Y.; Zang, C.; Li, Q.; Jiang, B. Experimental Investigation on Pressure Relief Mechanism of Specimens with Prefabricated Reaming Boreholes. *Rock Mech. Rock Eng.* **2023**, *56*, 2949–2966. [CrossRef]
36. Chen, M.; Zang, C.; Ding, Z.; Zhou, G.; Jiang, B.; Zhang, G.; Zhang, C. Effects of confining pressure on deformation failure behavior of jointed rock. *J. Cent. South Univ.* **2022**, *29*, 1305–1319. [CrossRef]
37. Chen, M.; Yang, L.; Zang, C.; Chen, Y.; Qi, Z.; Kong, B. Study on mechanical behavior and failure mechanism of specimens with single joint subjected to dynamic cyclical loading. *Fatigue Fract. Eng. Mater. Struct.* **2023**, *46*, 2878–2894. [CrossRef]
38. Liu, Z.; Liu, K.; Chen, X.; Ma, Z.; Lv, R.; Wei, C.; Ma, K. Deep-sea rock mechanics and mining technology: State of the art and perspectives. *Int. J. Min. Sci. Technol.* **2023**, *33*, 1083–1115. [CrossRef]
39. Lin, F.; Huang, R. Discussion on the limit equilibrium method of slope stability. *J. Geol. Hazards Environ. Preserv.* **1997**, *4*, 9–13.
40. Lu, Y.; Wang, S. The application of arc strip method in the stability of rock slope. *J. Xi'an Polytech. Univ.* **2010**, *24*, 619–622.
41. Zheng, Y.; Zhao, S.; Zhang, L. Using finite element strength reduction method to analyze slope stability. *Strateg. Study CAE* **2002**, *10*, 57–61+78.
42. Israr, M.K.; Shuhong, W. Slope Stability Analysis to Correlate Shear Strength with Slope Angle and Shear Stress by Considering Saturated and Unsaturated Seismic Conditions. *Appl. Sci.* **2021**, *11*, 4568.
43. Lysandros, P.; Elias, G.; Paraskevas, K.G. Stability assessment of soil slopes in three dimensions: The effect of the width of failure and of tension crack. *Geomech. Eng.* **2020**, *22*, 319–328.
44. Park, D.; Michalowski, L.R. Three-dimensional stability analysis of slopes in hard soil/soft rock with tensile strength cut-off. *Eng. Geol.* **2017**, *229*, 73–84. [CrossRef]
45. Zhang, Y.C.; Yang, G.H.; Hu, H.Y.; Liu, P. Method to Identify the Critical Slip Surface of Side Slope via the Deformation Field and Stress Field Calculated through Deformation Modulus Elastoplasticity Strength Reduction Method. *Appl. Mech. Mater.* **2011**, *90–93*, 3–11. [CrossRef]
46. Wu, Z.; Hu, Y.; Yang, H. Research Progress of Strength Reduction Method in Analysis of Slope Stability. *J. Shaoxing Univ. Nat. Sci.* **2019**, *39*, 28–37+2.
47. Yuan, W.; Li, X.; Bai, B.; Shi, L. A strength reduction method considering tensile failure. *Chin. J. Rock Mech. Eng.* **2014**, *33*, 3009–3014.
48. Zheng, H.; Li, C.; Li, C.; Ge, X. Finite element method for solving the factor of safety. *Chin. J. Geotech. Eng.* **2002**, *5*, 626–628.
49. Wang, H.; Gao, Y.; Jin, A.; Zhang, K. Determination of stiffness parameters of jointed rock masses with 3DEC simulations. *Chin. J. Rock Mech. Eng.* **2014**, *33*, 2894–2900.
50. Wu, C.; Chen, Z. Stability Analysis of Triangular Body of High Rock Slope Based on 3DEC. *J. Gansu Sci.* **2019**, *31*, 24–29.

51. Chen, N. *Experimental Research on Anisotropic Mechanical Behavior of Weak Rocks with Lamellar Fabric*; School of Architecture and Civil Engineering of Hubei University of Technology: Wuhan, China, 2020; pp. 1–56.
52. Wang, Z.; Ma, S.; Yuan, H.; Yuan, H.; Liu, X.; Zhai, R. Stability evaluation and reinforcement effect analysis of mica quartz schist slope on Xiasha expressway. *Subgrade Eng.* **2018**, 238–243. [CrossRef]